Bollettino della Società Paleontologica Italiana, 65 (2), 2026, 143-161. Modena

Early biomineralization in conodonts

Annalisa Ferretti*, Manuel Rigo, Federico Lugli, Przemysław Lech Świś, Daniele Malferrari, Thomas Letulle & Luca Medici

A. Ferretti, Dipartimento di Scienze Chimiche e Geologiche, Università degli Studi di Modena e Reggio Emilia, via Campi 103, I-41125 Modena, Italy; ferretti@unimore.it **corresponding author*
M. Rigo, Dipartimento di Geoscienze, Università di Padova, via G. Gradenigo 6, I-35131 Padova, Italy; manuel.rigo@unipd.it
F. Lugli, Dipartimento di Scienze Chimiche e Geologiche, Università degli Studi di Modena e Reggio Emilia, via Campi 103, I-41125 Modena, Italy; federico.lugli@unimore.it
P.L. Świś, Dipartimento di Scienze Chimiche e Geologiche, Università degli Studi di Modena e Reggio Emilia, via Campi 103, I-41125 Modena, Italy; swis.przemyslaw@gmail.com
D. Malferrari, Dipartimento di Scienze Chimiche e Geologiche, Università degli Studi di Modena e Reggio Emilia, via Campi 103, I-41125 Modena, Italy; daniele.malferrari@unimore.it
T. Letulle, Dipartimento di Geoscienze, Università di Padova, via G. Gradenigo 6, I-35131 Padova, Italy; thomasletullegeoc@gmail.com
L. Medici, CNR (Consiglio Nazionale delle Ricerche), IMIOT (Istituto di Metodologie Integrate per l'Osservazione della Terra), I-85050 Tito Scalo (Potenza), Italy; luca.medici@cnr.it

KEY WORDS - Bioapatite, paraconodonts, euconodonts, unit-cell parameters, Crystallinity Index.

ABSTRACT - Conodonts represent the earliest vertebrate group to have developed extensively mineralized tissues, providing a unique record of the early evolution of vertebrate biomineralization. Herein, we investigate the crystallographic differences between paraconodonts and euconodonts through an integrated characterization of their bioapatite structure. A broad dataset of conodont elements ranging from the Cambrian to the Triassic was investigated by electron microscopy and X-ray microdiffraction, with particular emphasis on bioapatite unit-cell parameters, Crystallinity Index (CI) and number of coherently diffracting unit-cell repeats. Taken together, the investigated parameters reveal distinct crystallographic distributions for paraconodonts and euconodonts. Paraconodonts occupy a comparatively restricted crystallographic field, characterized by lower a *and higher* c *unit-cell parameters, smaller unit-cell volumes, lower CI values, and smaller crystallite dimensions, whereas euconodonts show generally higher crystallinity and substantially greater crystallographic variability. Although carbonate content was not measured directly, the unit-cell differences are consistent with higher carbonate content in paraconodont bioapatite. Differences in crystallite development along the* ***a*** *and* ***c*** *axes further suggest that the transition to the euconodonts did not involve a simple increase in crystallinity or isotropic crystal growth, but rather a reorganization of apatite at the crystallographic scale. No clear differences were detected between basal and denticle regions in selected euconodonts, and CI showed no clear association with the conodont Color Alteration Index (CAI). The group-level crystal-chemical differences may retain a biological component, although unequal sample sizes, taxonomic composition, and diagenetic variability limit its isolation. Remarkably, the mineralogical differences identified herein between paraconodont and euconodont bioapatite parallel those distinguishing dentine and enamel/enameloid in more advanced vertebrates. More specifically, qualitative comparison with differentiated dental tissues of fossil and extant catsharks reveals partial correspondence between paraconodonts and shark roots and between euconodonts and shark crowns, although these similarities do not imply tissue homology. This correspondence suggests that the transition from paraconodont to euconodont mineralization may have captured an early stage in the differentiation and specialization of vertebrate mineralized tissues, potentially providing insight into the emergence of distinct tissue types during the early evolution of the vertebrate skeleton.*

INTRODUCTION

Conodonts are an extinct group of jawless vertebrates with a fossil record spanning more than 300 million years, from the Cambrian to the Early Jurassic transition (Du et al., 2020, 2023; Ferretti et al., 2020; Corradini et al., 2026). They were soft-bodied animals characterized by a feeding apparatus generally composed, with only a few known exceptions (Liu et al., 2017), of 15-19 mineralized elements arranged in a bilaterally symmetrical pattern (e.g., Aldridge et al., 1995; Purnell et al., 2000). From an evolutionary perspective, conodonts are particularly significant because they represent the earliest vertebrate group to have developed extensive skeletal biomineralization (Murdock et al., 2013). Their abundant fossil record and the mineralized nature of their feeding elements therefore provide an exceptional archive for investigating the early evolution of vertebrate hard tissues and their subsequent alteration during fossilization.

A fundamental distinction in the early history of conodont biomineralization is that between paraconodonts and euconodonts. Paraconodonts occur predominantly in Cambrian successions and are characterized by comparatively simple elements, whereas euconodonts developed more complex feeding apparatuses and a highly differentiated architecture of their mineralized tissues (Fig. 1). Although the evolutionary relationships between these groups have long been discussed (see a brief summary below), paraconodonts are particularly relevant for understanding the emergence and progressive specialization of conodont hard tissues. As detailed below, the transition toward the euconodonts involved not only morphological changes but also substantial differences in the organization and mineralization of the elements, making the comparison between paraconodont and euconodont bioapatite especially informative for investigating the biological control exerted on early vertebrate biomineralization.

ISSN 0375-7633 doi:10.4435/BSPI.2026.08

The aim of the present study is to investigate potential crystallographic differences between paraconodonts and euconodonts by applying an analytical protocol routinely employed by our research group. Previous crystallographic investigations have shown that paraconodont and euconodont bioapatite occupy distinct fields in terms of bioapatite unit-cell parameters (Medici et al., 2020; Ferretti et al., 2021), suggesting that differences in tissue organization may also be expressed at the crystal-chemical scale. However, the euconodont dataset previously analyzed offered scope for further refinement and expansion. We therefore broadened the dataset by incorporating additional material, primarily of Silurian and Devonian age (e.g., Corradini et al., 1998; Świś et al., 2026). In addition, building on recent studies demonstrating that complementary descriptors can separate biological signatures from post-mortem alterations, we analyzed two further parameters, the Crystallinity Index and $N_{UnitCell}$, to assess the number of coherently diffracting unit-cell repeats and their directional organization. This allowed us to test whether the transition to the euconodonts was accompanied by systematic changes in apatite organization. Moreover, comparing these metrics with root and crown tissues from fossil and extant catsharks allowed us to test whether the paraconodont-euconodont transition involved a broader bioapatite reorganization linked to tissue differentiation, while also accounting for potential diagenetic overprinting. This approach is intended to provide further insights into the role of bioapatite in the earliest biomineralization processes involving organisms starting from the Cambrian.

HARD TISSUES IN CONODONTS

The affinity and role of Cambrian conodonts in the evolutionary history of the group have long been debated. Bengtson (1976, p. 185) stated that: "During most of their time span, conodonts constitute a structurally coherent group, and usually it is not difficult to recognize that they are conodonts. Early in their history, however, the point is altogether less clear; there are many phosphatic problematical fossils in Cambrian rocks which have been suggested, usually with some reservation, to be possibly related to conodontophorids and perhaps even ancestral to them."

Building on two decades of discoveries that had extended the conodont record back into the Cambrian, Bengtson (1976) undertook a detailed study of Cambrian conodont material. A few years before, Müller (1962) had introduced the order Paraconodontida to accommodate some of these forms and proposed that their elements grew through basal accretion, although he did not explicitly assign them to the true conodonts. However, Bengtson (1976) refrained from using Paraconodontida as a formal systematic group because the phylogenetic relationships among the forms assigned to it were poorly understood. Instead, he adopted the informal term "paraconodonts" for forms sharing the structural organization defined by Müller & Nogami (1971, 1972) through conventional light-microscopic examination of thin sections, without implying that they necessarily belonged to a single evolutionary lineage. In addition, Bengtson (1976) introduced the term "euconodont" for elements consisting of two distinct components: what he called the "conodont proper" and the basal body. The conodont proper is characterized by successive lamellae externally superimposed on one another that are continuous around the tips of the denticles. Today, this is usually called the conodont crown. The basal body is likewise composed of lamellae, although these are not always continuous around the base of the conodont element. In contrast, paraconodont elements show no clear differentiation between a basal body and a conodont proper. Bengtson (1976, p. 200) also introduced the term protoconodonts: "Protoconodonts are forms with deep internal cavities and with growth lamellae added only at the inner surface; there is no evidence of external deposition of lamellae." According to Bengtson (1976, 1983), proto-, para-, and euconodonts would represent successive stages within a single evolutionary lineage. As elegantly summarized by Donoghue (1998), protoconodonts were subsequently recognized as a distinct group of organisms (Chaetognathans; Szaniawski, 1982), whereas the proposed evolutionary relationship between paraconodonts and euconodonts continued to receive support.

According to Pietzner et al. (1968), the basal body and conodont proper share the same mineralogical composition, although the basal body is characterized by smaller and more nearly isodiametric crystallites. Later, Müller & Nogami (1972) showed that paraconodonts are composed of very fine crystallites, making their microstructure more comparable to that of the euconodont basal body than to the conodont proper.

Following the discovery of the soft body of conodonts, investigations of structural differences among conodont elements increasingly shifted toward a biological perspective, with particular emphasis on understanding the significance of variations in their mineralized tissues. Moreover, histological evidence became a key tool for assessing the biological affinities of conodonts and clarifying their phylogenetic position.

Donoghue (1998) provided a detailed characterization of conodont element ultrastructure through the combined use of thin sections, naturally and experimentally fractured specimens, and several imaging techniques, including scanning electron microscopy, incident and transmitted light microscopy, and laser confocal microscopy. Lamellar tissue generally constitutes the predominant component of the element and is distinguished from other conodont hard tissues by its comparatively coarse crystalline organization. Crystal dimensions are highly variable, although most crystallites are only a few micrometers long, with a broader range extending from less than 1 μm to more than 30 μm. Beneath the crown, the basal body consists of a single type of hard tissue that preserves distinct growth striae and has a much finer crystalline structure than the crown tissue, to the extent that individual crystallites cannot normally be resolved using light microscopy. Basal tissue exhibits considerable structural variability, not only among different conodont taxa but also within individual taxa (Donoghue, 1998).

The same author also investigated potential homologies between conodont mineralized tissues and those of chordates, with particular emphasis on the proposed correspondence of lamellar crown tissue with enamel or

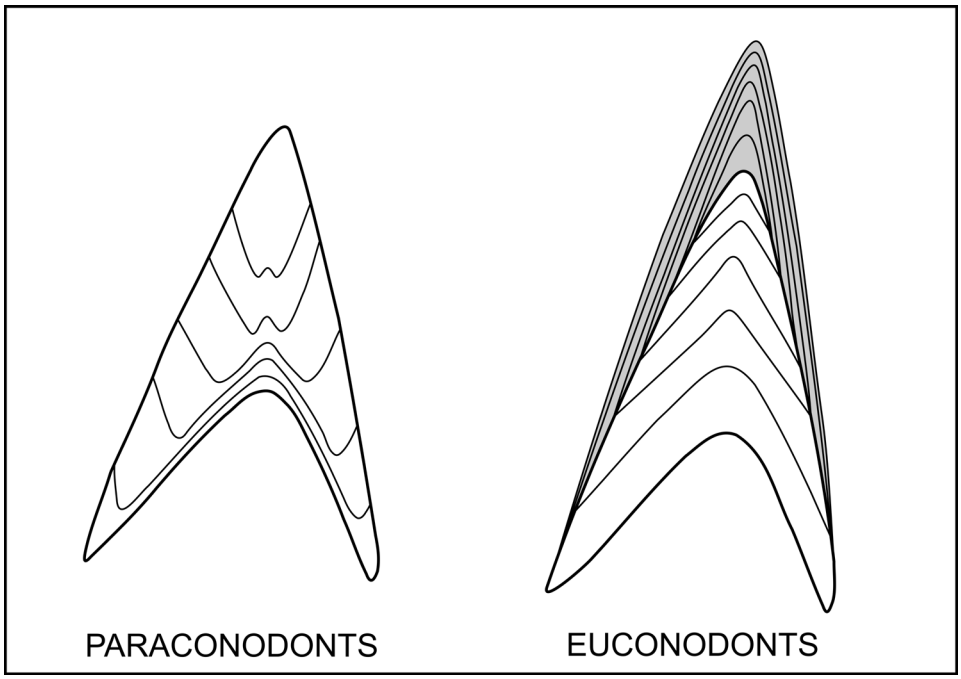

Fig. 1 - Tissue organization in paraconodonts and euconodonts. Paraconodont elements are composed of a single tissue type displaying distinct incremental growth lines that form a series of hollow, cone-shaped laminae. In contrast, euconodont elements contain two tissue types: a basal body (white), which exhibits a growth pattern comparable to that of paraconodont elements, and a distinct crown (gray) (redrawn after Murdock et al., 2014).

enameloid. Although both vertebrate tissues are highly mineralized, they exhibit distinct patterns of crystallite organization. Enameloid is generally characterized by relatively large, elongate crystallites, often fiber-like in morphology, whose arrangement may range from strongly oriented to essentially random. Enamel, by contrast, consists of smaller crystallites, typically associated with incremental growth lines and displaying a preferential orientation that is commonly approximately perpendicular to the growing surface, although some variability may occur. Based on these microstructural features, Donoghue (1998) concluded that conodont lamellar crown tissue exhibits a greater structural similarity to enamel than to enameloid, supporting the interpretation of lamellar crown tissue and enamel as homologous tissues. According to Donoghue (1998), the distinct growth relationship between basal tissue and enamel provides additional support for interpreting conodont basal tissue as potentially homologous to bone, mineralized cartilage, or dentine. White matter, in turn, is interpreted as a conodont-specific tissue with affinities to dentine, showing its closest resemblance to primitive mesodentine. This comparison is nevertheless imperfect, as white matter lacks the pulp canals that commonly characterize mesodentine. The enamel-dentine association and their appositional pattern of growth identify the denticle as an odontode-like developmental unit (Donoghue, 1998).

Sansom et al. (1994) made a major contribution to this debate through detailed histological examination of thin sections of euconodont elements. In particular, they recognized two distinct forms of dentine within the basal body: one characterized by scalloped growth lines associated with traces of tubules oriented approximately perpendicular to them, and another displaying a network of branching tubules. These microstructural features were regarded as diagnostic of vertebrate dentine, providing strong evidence for the vertebrate affinity of conodonts and playing a decisive role in resolving the long-standing debate concerning their biological affinities and systematic position (Sansom et al., 1994). Two years later, Sansom (1996) documented the presence of both enamel and dentine in *Pseudooneotodus*, occurring in the crown and basal body, respectively. Importantly, these tissue types were recognized in specimens spanning the entire known stratigraphic range of the genus, from the Ordovician to the Devonian. However, it is worth emphasizing that *Pseudooneotodus* represented a particularly intriguing case, as its assignment to the conodonts had been the subject of considerable debate and uncertainty in earlier studies.

Murdock et al. (2013) investigated the proposed evolutionary relationship between paraconodonts and euconodonts using synchrotron radiation X-ray tomographic microscopy to compare the microstructure of morphologically similar paraconodont and euconodont elements. Their results revealed different degrees of tissue differentiation among paraconodonts, including structural features and growth patterns comparable to those of euconodont basal bodies. This variation was interpreted as evidence for the progressive, stepwise acquisition of characteristic euconodont features, supporting a paraconodont ancestry for euconodonts. Importantly, this evolutionary scenario challenges the previously proposed homology between euconodont crown tissue and vertebrate enamel, implying that these tissues originated independently. Consequently, the close ontogenetic, structural, and topological correspondence between conodont elements and vertebrate odontodes is

interpreted by Murdock et al. (2013) as an example of convergent evolution rather than a common evolutionary origin. Under this evolutionary scenario, the common ancestor of conodonts and jawed vertebrates is inferred to have lacked a mineralized skeleton, but to have possessed genetic preadaptations that were independently exploited by both groups at different times in their evolutionary histories.

Murdock et al. (2014) subsequently investigated the functional consequences of this tissue differentiation using finite-element analyses of morphologically comparable paraconodont and euconodont elements. Their models separated the effects of element shape from those of tissue composition and showed that morphology, particularly basal-cavity depth and cusp thickness, strongly influences stress distribution. More importantly, the development of a relatively stiff euconodont crown over a more compliant basal tissue substantially reduced deformation and strain under equivalent loading. The crown therefore provided a mechanical advantage in addition to previously proposed benefits such as, for example, abrasion resistance, preservation of functional morphology during episodic growth, and increased capacity for ontogenetic modification (Murdock et al., 2014). Progressive thickening of the crown tissue and reduction of the basal cavity may have further decreased stresses within the basal body and possibly contributed to the increasing morphological and functional disparity of euconodonts, potentially facilitating their ecological radiation and the full replacement of paraconodonts during the late Cambrian and the Early Ordovician.

The combined results of Murdock et al. (2013, 2014) therefore support a model in which conodont and gnathostome dental tissues evolved independently under similar functional constraints. Although the euconodont crown and vertebrate enamel are not homologous under this interpretation, both represent stiff, highly mineralized outer tissues that improve mechanical performance and protect underlying, more compliant tissues. Their similarity is thus interpreted as the product of convergent functional selection rather than inheritance from a common mineralized odontode system (Murdock et al., 2013, 2014).

Recent work has further refined this broader context. Haridy et al. (2025) reassessed *Anatolepis*, a Cambrian-Ordovician phosphatic fossil previously interpreted as preserving the earliest vertebrate dentine, and showed through high-resolution synchrotron analyses that the putative dentine tubules are instead sensory structures of an arthropod exoskeleton. This shifts the earliest unequivocal evidence of vertebrate dental tissues to the Middle Ordovician and reinforces the distinctiveness of the conodont biomineralization system, which represents one of the earliest examples of vertebrate mineralization but lacks true dentine (Haridy et al., 2025). Similarly, synchrotron-based analyses of the Silurian jawless vertebrates *Jamoytius* and *Lasanius* have documented apatitic biomineralization and suggest that bone originated close to, or possibly before, the origin of the vertebrate crown group (Reeves et al., 2026).

Taken together, all these studies clearly emphasize that early vertebrate biomineralization followed multiple tissue architectures and possibly even diverse evolutionary trajectories, among which the conodont mineralized skeleton represents an early and highly distinctive system.

A CRYSTALLOGRAPHIC APPROACH TO CONODONT BIOAPATITE

Bioapatite is a nanocrystalline biomineral that played a fundamental role in vertebrate evolution by enabling the development of mineralized skeletal and dental tissues. Bioapatite is structurally related to minerals of the apatite group, which commonly crystallize in the hexagonal system and include several abiotic end-members. This biogenic phase is commonly represented by the simplified general formula $Ca_5(PO_4,CO_3)_3(F,OH)$. One of its most distinctive features is its pronounced crystal-chemical flexibility, which allows numerous isovalent and heterovalent chemical substitutions at both cationic and anionic sites. Such substitutions may originate during biologically mediated mineralization or be introduced or modified after death through burial and diagenetic processes. Fossil bioapatite can consequently preserve a complex combination of primary biological information and secondary environmental and diagenetic signals (e.g., Malferrari et al., 2019; Michailow et al., 2025).

This interplay between biological control and post-mortem modification is particularly relevant when paraconodont and euconodont bioapatite are compared. Differences in the organization and differentiation of their mineralized tissues raise the possibility that their crystal lattices retain a component inherited from primary biomineralization, even after burial-related modification. At the same time, crystal-chemical investigations have shown that fossilization may modify bioapatite unit-cell parameters (Ferretti et al., 2021), whereas secondary apatite overgrowths may closely replicate the unit-cell parameters of older conodont apatite (Ferretti et al., 2017). Crystallographic similarities or differences in fossil conodont apatite therefore cannot, in isolation, be attributed unequivocally either to biological affinity or to diagenetic modification. Instead, they may reflect the superposition of primary mineralization patterns and subsequent post-mortem transformations.

A further component of this structural record is crystallinity, considered here in a broad sense as the degree and spatial extent of structural coherence within bioapatite. Rather than being represented by a single parameter, crystallinity can be assessed using complementary descriptors. Medici et al. (2026), in their comparative crystallographic investigation of Recent and fossil catshark teeth and scales, evaluated several such parameters as potential indicators of biological signatures and post-mortem modifications. Among these, the Crystallinity Index (CI) provides an operational measure of crystalline organization based on diffraction-peak characteristics, whereas $N_{UnitCell}$ expresses the approximate number of coherently diffracting unit-cell repeats along a given crystallographic direction and, therefore, provides directional information on coherent-domain development (the definitions of CI and $N_{UnitCell}$, together with the procedures used for their calculation, are provided in the Methods section). Both descriptors may reflect aspects of the original organization of

mineralized tissues as well as structural modifications occurring during fossilization. CI has already been used as an indirect indicator of recrystallization and diagenetic alteration (e.g., Person et al., 1995; Pucéat et al., 2004; Trueman et al., 2008), but neither CI nor $N_{UnitCell}$ should be regarded as a direct or unambiguous proxy for diagenetic intensity. The relationship between CI and alteration may be complex and method-dependent (Medici et al., 2021), and the same caution applies to $N_{UnitCell}$, which describes coherent-domain development rather than diagenetic overprint (Medici et al., 2026). CI values can be influenced by coherent-domain size, lattice strain, sample texture, preferred crystallographic orientation, chemical substitutions within the apatite lattice, and the method used for its calculation (Trueman et al., 2008; Medici et al., 2021). Estimates of coherent-domain dimensions, and hence $N_{UnitCell}$ values, also depend on peak fitting, correction for instrumental broadening, and the assumptions adopted in diffraction-line-broadening analysis (Medici et al., 2026).

During fossilization, degradation and loss of the organic matrix may facilitate reorganization and growth of the inorganic crystalline fraction, potentially producing changes in CI, coherent-domain dimensions and corresponding $N_{UnitCell}$ values, as well as in unit-cell dimensions. However, these variables need not change in parallel because they describe different aspects of the apatite structure. Changes in unit-cell parameters and volume additionally depend on the type and extent of carbonate incorporation, other chemical substitutions, and structural modifications affecting the bioapatite lattice. Consequently, crystallinity descriptors and unit-cell dimensions should be interpreted jointly, rather than individually, when assessing the relative contributions of original biological organization and post-mortem alteration.

Trace-element signatures, including REE and HFSE distributions, may provide complementary information on fluid-apatite interactions and diagenetic overprinting (e.g., Medici et al., 2021, 2026). However, their investigation requires a dedicated geochemical dataset and lies outside the objectives of the present study; accordingly, REE and HFSE data are neither analyzed nor used for comparative purposes here. Instead, we focus specifically on unit-cell parameters, CI, and the directional development of coherent domains, evaluated through their apparent dimensions and corresponding $N_{UnitCell}$ values, to assess whether paraconodonts and euconodonts retain distinct crystallographic signatures and to explore their possible relationship to tissue differentiation. Comparison with root and crown tissues of fossil and Recent catsharks provides an additional comparative crystallographic framework for discussing broader patterns of vertebrate biomineralization.

MATERIALS

The core of the analyzed material consisted of specimens previously investigated by Medici et al. (2020), supplemented by additional material from various sources to assemble a broad and taxonomically diverse dataset suitable for the purposes of the present study (Pl. 1). Most specimens were obtained from well-known and previously published stratigraphic sections with robust biostratigraphic constraints, allowing them to be confidently assigned to specific time intervals. With regard to the Late Ordovician, conodont faunas from several European regions have been extensively documented, including the Carnic Alps (Bagnoli et al., 1998; Ferretti et al., 2025), Ireland (Ferretti et al., 2014b), Sardinia (Ferretti & Serpagli, 1999), Normandy (Ferretti et al., 2014a), and northern England (Bergström & Ferretti, 2015). The strong predominance of Upper Ordovician material reflects a specific research approach, as these specimens had been extensively investigated to evaluate the potential effects of taxonomy, element position within the feeding apparatus, and geographic provenance on the analyzed parameters (Medici et al., 2020). Within this broader framework, the material selected for the present study encompasses a taxonomically and geographically diverse range of conodont elements spanning different CAI values (1-6), thereby allowing crystallographic patterns to be assessed across specimens characterized by different thermal histories. Material investigated herein derives from several sources, reflecting both the long-standing tradition of conodont research at the University of Modena and Reggio Emilia (Italy) and the contributions of previous and ongoing studies conducted by our research group (see Introduction). A substantial portion of the specimens belongs to the historical conodont collections assembled by Enrico Serpagli over the course of his career and currently incorporated into the Paleontological Collections of the University of Modena and Reggio Emilia, Italy (IPUM Collection). As mentioned above, these collections were complemented by material previously prepared and analyzed within the framework of earlier studies carried out by members of our research group, as well as by additional specimens generously provided by colleagues and other conodont researchers.

The resulting dataset comprises 126 conodont elements (Tab. 1), spanning a wide stratigraphic interval from the Cambrian to the Triassic, including both paraconodonts and euconodonts. Such a broad temporal coverage was selected to encompass major stages in conodont evolutionary history and to provide a representative framework for investigating variation in the structural and compositional characteristics of conodont hard tissues.

All analyzed specimens are housed in the Paleontological Collections (IPUM) of the Department of Chemical and Geological Sciences, University of Modena and Reggio Emilia, Modena, Italy, where they are permanently curated and available for future reference and comparative studies.

METHODS

SEM/ESEM microscopy

Conodont elements were initially examined and documented using optical and electron microscopy at the University of Modena and Reggio Emilia (Modena, Italy). Specimens were mounted on aluminum stubs covered with carbon-conductive adhesive tape and examined either Au-coated or uncoated. Electron-microscopy observations were performed using an FEI ESEM Quanta

200 Environmental Scanning Electron Microscope (ESEM), equipped with an Oxford EDX INCA 300 energy-dispersive X-ray spectrometer, and an FEI Nova NanoSEM 450 Scanning Electron Microscope (SEM), equipped with a Bruker QUANTAX-200 XEDS detector. ESEM analyses were conducted under both high- and low-vacuum conditions (0.5-1 Torr), using accelerating voltages of 5-25 keV for imaging and 5-15 keV for elemental analyses. SEM observations were performed under high-vacuum conditions, with accelerating voltages of 15-25 keV for both imaging and elemental analyses.

X-ray microdiffraction (μ-XRD)

X-ray microdiffraction (μ-XRD) is a versatile technique that enables the non-destructive characterization of structural properties, including the mineralogical composition of crystalline phases, degree of crystallinity, crystallite size, and preferential orientation. μ-XRD provides accuracy comparable to that of conventional diffractometers while allowing measurements to be performed on very small areas, making it particularly suitable for the analysis of small fossil specimens.

Specimens suitable for analysis (Tab. 1) were characterized at the Institute of Methodologies for Environmental Analysis of the National Research Council of Italy in Tito Scalo (Potenza, Italy), following the protocols previously established and validated by Ferretti et al. (2017, 2021, 2023), Malferrari et al. (2019, 2024), and Medici et al. (2020, 2021, 2026). A representative subset of specimens (indicated by underlined sample codes in Tab. 1) was further selected for measurement and calculation of the CI. The μ-XRD measurements were carried out on elements mounted on small, flat surfaces using a Rigaku D/MAX RAPID diffraction system operating at 40 kV and 30 mA. The instrument was equipped with a CuKα radiation source, a curved

EXPLANATION OF PLATE 1

SEM images of some of the conodont elements analyzed in this study. All elements refigured after Medici et al. (2020) except 1, 3, 7, 11-14 (this study) and 15, 18 and 21 (refigured after Świś et al., 2026). Scale bars correspond to 200 μm.

Figs 1-2 - *Furnishina* sp., late Cambrian, specimens no. A13 and A14, IPUM 35381 and IPUM 29103, respectively, Västergötland (Sweden).

Figs 3-4 - *Westergaardodina* sp., late Cambrian, specimens no. A12 and A11, IPUM 35382 and IPUM 29101, respectively, Västergötland (Sweden).

Figs 5, 7 - *Furnishina alata* Szaniawski, 1971, late Cambrian, specimens no. A18 and A19, IPUM 29102 and IPUM 35383, respectively, Żarnowiec (Poland).

Fig. 6 - *Rhipidognathus symmetricus* Branson, Mehl & Branson, 1951, Late Ordovician, specimen no. A22, IPUM 29109, Saluda Dolomite (USA).

Figs 8-9 - *Amorphognathus* sp., Late Ordovician, specimens no. A27 and A98, IPUM 29107 and IPUM 29111, respectively, Westmorland (UK).

Fig. 10 - *Paltodus deltifer deltifer* (Lindström, 1955), Early Ordovician, specimen no. A6, IPUM 29104, Öland (Sweden).

Fig. 11 - *Icriodella* sp., Late Ordovician, specimen no. 21, IPUM 35384, Normandy (France).

Fig. 12 - *Wurmiella excavata* (Branson & Mehl, 1933), Silurian, specimen no. 59, IPUM 35385, Carnic Alps (Austria).

Fig. 13 - *Dapsilodus obliquicostatus* (Branson & Mehl, 1933), Silurian, specimen no. 57, IPUM 35386, Carnic Alps (Austria).

Fig. 14 - *Scabbardella altipes* (Henningsmoen, 1948), Late Ordovician, specimen no. A54, IPUM 35387, Normandy (France).

Fig. 15 - *Branmehla* sp., Late Devonian, specimen no. S01, IPUM 35362, Dzikowiec (Poland).

Fig. 16 - *Lanea omoalpha* (Murphy & Valenzuela-Ríos, 1999), Early Devonian, specimen no. A2, IPUM 29108, U Topolů (Bohemia).

Fig. 17 - *Palmatolepis subperlobata* Branson & Mehl, 1934, Late Devonian, specimen no. A102, IPUM 29118, Texas (USA).

Fig. 18 - *Bispathodus* sp., Late Devonian, specimen no. S010, IPUM 35369, Sardinia (Italy).

Fig. 19 - *Zieglerodina planilingua* (Murphy & Valenzuela-Ríos, 1999), Early Devonian, specimen no. A1, IPUM 29112, U Topolů (Bohemia).

Fig. 20 - *Palmatolepis triangularis* Sannemann, 1955, Late Devonian, specimen no. A101, IPUM 29117, Texas (USA).

Fig. 21 - *Palmatolepis* sp., Late Devonian, specimen no. S017, IPUM 35377, Kowala (Poland).

Fig. 22 - *Gnathodus* sp., Middle Mississippian, specimen no. A78, IPUM 29115, Carnic Alps (Italy).

Figs 23, 25 - *Pachycladina obliqua* Staesche, 1964, Early Triassic, specimens no. A87 and A86, IPUM 29119 and IPUM 29121, respectively, Dolomites (Italy).

Fig. 24 - Unrecognizable fragment, Early Mississippian, specimen no. A77, IPUM 29120, Carnic Alps (Italy).

Figs 26-27 - *Carnepigondolella pseudodiebeli* (Kozur, 1972), Late Triassic, specimens no. A44 and A43, IPUM 29123 and IPUM 29124, respectively, Sicily (Italy).

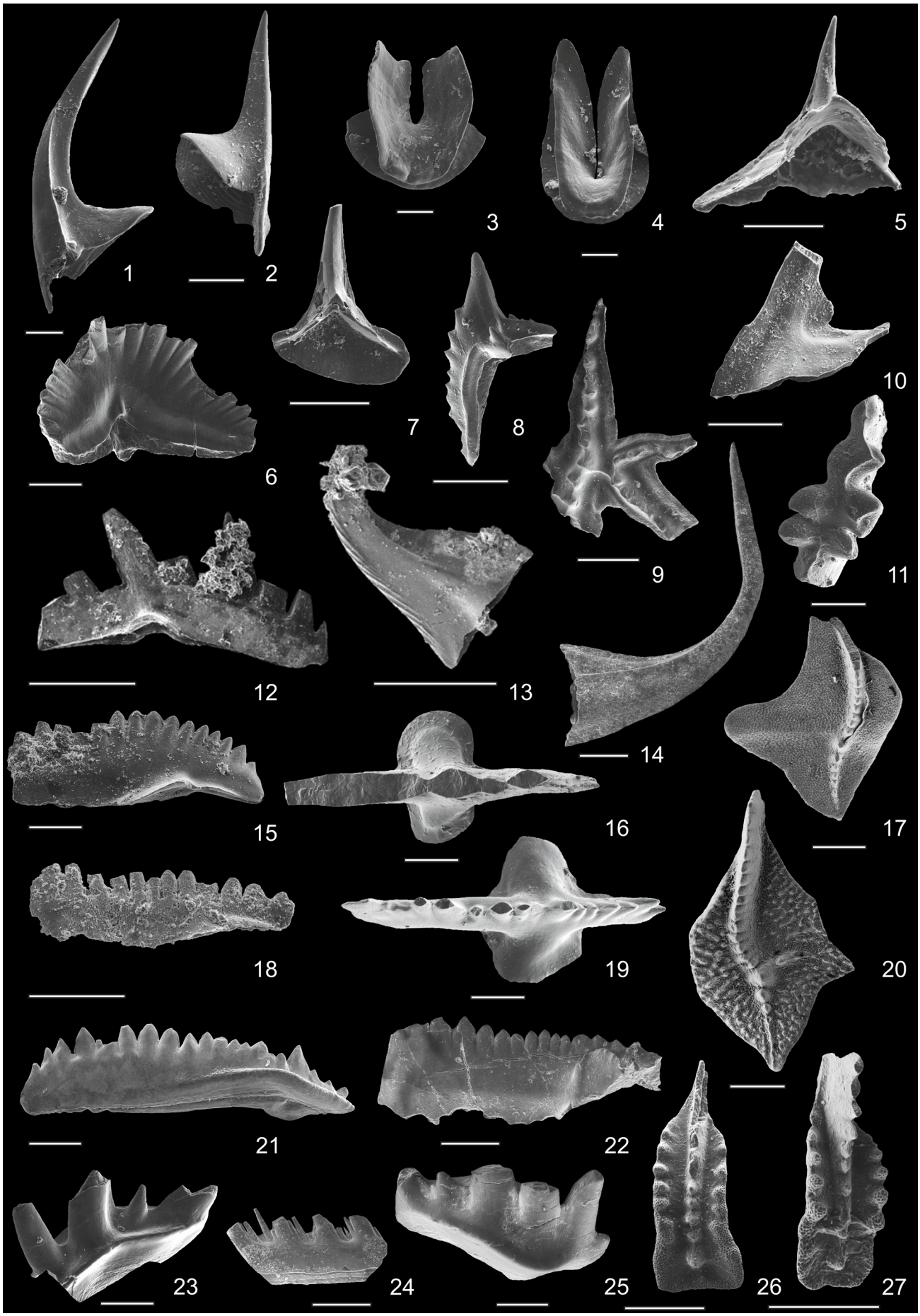
1
2
3
4
5
6
7
8
9
10
11
12
13
14
15
16
17
18
19
20
21
22
23
24
25
26
27

CODE	N° ELEMENTS	CONODONT TAXA	LOCALITY	SYSTEM/SERIES (STAGE)	P/E	CAI	REFERENCE PAPER(S)/ COLLECTION
A18-A19	2	*Furnishina alata* Szaniawski, 1971	Żarnowiec (Poland)	Cambrian/ Miaolingian (Guzhangian)	P		Szaniawski (1971)
A11-A12, A90-A91	4	*Westergaardodina* sp.	Västergötland (Sweden)	Cambrian/ Furongian (Paibian)	P		Müller & Hinz (1991)
A13-A14, A88-A89, A110	5	*Furnishina* sp.	Västergötland (Sweden)	Cambrian/ Furongian (Paibian)	P		Müller & Hinz (1991)
A15	1	unrecognizable fragment	Västergötland (Sweden)	Cambrian/ Furongian (Paibian)	P		Müller & Hinz (1991)
A5-A6	2	*Paltodus deltifer deltifer* (Lindström, 1955)	Öland (Sweden)	Lower Ordovician (Tremadocian)	E	1.5	IPUM Collection
A10	1	unrecognizable fragment	Öland (Sweden)	Lower Ordovician (Tremadocian)	E	1.5	IPUM Collection
A20-A21	2	*Paltodus deltifer pristinus* (Viira, 1970)	Northern Estonia	Lower Ordovician (Tremadocian)	E	1.5	Viira (1970)
A30-A31, A98-A99	4	*Amorphognathus* sp. (Pa)	Westmorland (UK)	Upper Ordovician (Katian)	E	4	Bergström & Ferretti (2015)
A27-A29	3	*Amorphognathus* sp. (Pb)	Westmorland (UK)	Upper Ordovician (Katian)	E	4	Bergström & Ferretti (2015)
A32-A33-A34, A74-A75	5	*Scabbardella altipes* (Henningsmoen, 1948)	Westmorland (UK)	Upper Ordovician (Katian)	E	4	Bergström & Ferretti (2015)
A38, A66-A67	3	*Amorphognathus* sp. (Pa)	Sardinia (Italy)	Upper Ordovician (Katian)	E	5	Ferretti & Serpagli (1999)
A37, A41, A68, A72	4	*Amorphognathus* sp. (Pb)	Sardinia (Italy)	Upper Ordovician (Katian)	E	5	Ferretti & Serpagli (1999)
A39-A40, A69-A70	4	*Scabbardella altipes* (Henningsmoen, 1948)	Sardinia (Italy)	Upper Ordovician (Katian)	E	5	Ferretti & Serpagli (1999)
A49-A50-A51	3	*Amorphognathus* sp. (Pa)	Normandy (France)	Upper Ordovician (Katian)	E	4-5	Ferretti et al. (2014a)
62, A52, A107-A108	4	*Amorphognathus* sp. (Pb)	Normandy (France)	Upper Ordovician (Katian)	E	4-5	Ferretti et al. (2014a)
17	1	*Amorphognathus* sp. (Sd)	Normandy (France)	Upper Ordovician (Katian)	E	4-5	Ferretti et al. (2014a)
68, 82	2	*Hamarodus brevirameus* (Walliser, 1964) (M)	Normandy (France)	Upper Ordovician (Katian)	E	4-5	Ferretti et al. (2014a)
49	1	*Hamarodus brevirameus* (Walliser, 1964) (Sc)	Normandy (France)	Upper Ordovician (Katian)	E	4-5	Ferretti et al. (2014a)
21	1	*Icriodella* sp.	Normandy (France)	Upper Ordovician (Katian)	E	4-5	Ferretti et al. (2014a)
20, 56, A53	3	*Panderodus* sp.	Normandy (France)	Upper Ordovician (Katian)	E	4-5	Ferretti et al. (2014a)
24, 41	2	*Sagittodontina robusta* Knüpfer, 1967 (Pa)	Normandy (France)	Upper Ordovician (Katian)	E	4-5	Ferretti et al. (2014a)
46	1	*Sagittodontina robusta* Knüpfer, 1967 (Sd)	Normandy (France)	Upper Ordovician (Katian)	E	4-5	Ferretti et al. (2014a)
45, 59-60, 91, 103, A54, A109	7	*Scabbardella altipes* (Henningsmoen, 1948)	Normandy (France)	Upper Ordovician (Katian)	E	4-5	Ferretti et al. (2014a)
A22	1	*Rhipidognathus symmetricus* Branson, Mehl & Branson, 1951	Saluda Dolomite (USA)	Upper Ordovician	E	1	IPUM Collection
A23	1	*Panderodus* sp.	Saluda Dolomite (USA)	Upper Ordovician	E	1	IPUM Collection
A104	1	*Belodina* sp.	Missouri (USA)	Upper Ordovician	E	1	IPUM Collection

Tab. 1 - Conodont taxa analyzed in the present study, with their corresponding geographic provenance and/or geological formation, age, and literature describing the collection from which the material originates. The open nomenclature adopted for *Amorphognathus* reflects the presence of multiple species of the genus within the sample, which can be reliably distinguished only on the basis of the M element. For some samples in the UNIMORE collection, only the formation name was recorded, while the specific locality was not indicated. P, paraconodont; E, euconodont. Underlined numbers indicate the samples for which crystallinity indices have been calculated.

CODE	N° ELEMENTS	CONODONT TAXA	LOCALITY	SYSTEM/SERIES (STAGE)	P/E	CAI	REFERENCE PAPER(S)/ COLLECTION
A105	1	*Plectodina* sp.	Missouri (USA)	Upper Ordovician	E	1	IPUM Collection
A106	1	*Panderodus* sp.	Missouri (USA)	Upper Ordovician	E	1	IPUM Collection
56	1	*Dapsilodus obliquicostatus* (Branson & Mehl, 1933)	Carnic Alps (Austria)	Silurian/Ludlow	E	4	Schönlaub et al. (2017); Ferretti et al. (2023)
57	1	*Dapsilodus obliquicostatus* (Branson & Mehl, 1933)	Carnic Alps (Austria)	Silurian/Ludlow	E	4	Schönlaub et al. (2017); Ferretti et al. (2023)
58	1	*Dapsilodus obliquicostatus* (Branson & Mehl, 1933)	Carnic Alps (Austria)	Silurian/Ludlow	E	4	Schönlaub et al. (2017); Ferretti et al. (2023)
59	1	*Wurmiella excavata* (Branson & Mehl, 1933)	Carnic Alps (Austria)	Silurian/Ludlow	E	4	Schönlaub et al. (2017); Ferretti et al. (2023)
60	1	*Wurmiella excavata* (Branson & Mehl, 1933)	Carnic Alps (Austria)	Silurian/Ludlow	E	4	Schönlaub et al. (2017); Ferretti et al. (2023)
61	1	*Wurmiella excavata* (Branson & Mehl, 1933)	Carnic Alps (Austria)	Silurian/Ludlow	E	4	Schönlaub et al. (2017); Ferretti et al. (2023)
SF 50	1	*Pseudooneotodus beckmanni* Bischoff & Sannemann, 1958	Carnic Alps (Austria)	Silurian/Ludlow	E	4	Schönlaub et al. (2017); Ferretti et al. (2023)
SF 51	1	*Pseudooneotodus beckmanni* Bischoff & Sannemann, 1958	Carnic Alps (Austria)	Silurian/Ludlow	E	4	Schönlaub et al. (2017); Ferretti et al. (2023)
SF 52	1	*Pseudooneotodus beckmanni* Bischoff & Sannemann, 1958	Carnic Alps (Austria)	Silurian/Ludlow	E	4	Schönlaub et al. (2017); Ferretti et al. (2023)
SF 53	1	*Pseudooneotodus beckmanni* Bischoff & Sannemann, 1958	Carnic Alps (Austria)	Silurian/Ludlow	E	4	Schönlaub et al. (2017); Ferretti et al. (2023)
SF 54	1	*Pseudooneotodus beckmanni* Bischoff & Sannemann, 1958	Carnic Alps (Austria)	Silurian/Ludlow	E	4	Schönlaub et al. (2017); Ferretti et al. (2023)
SF 55	1	*Pseudooneotodus beckmanni* Bischoff & Sannemann, 1958	Carnic Alps (Austria)	Silurian/Ludlow	E	4	Schönlaub et al. (2017); Ferretti et al. (2023)
A1	1	*Zieglerodina planilingua* (Murphy & Valenzuela-Ríos, 1999)	U Topolů (Czech Republic)	Lower Devonian (Lochkovian)	E	3	Chlupáč et al. (1980)
A2	1	*Lanea omoalpha* (Murphy & Valenzuela-Ríos, 1999)	U Topolů (Czech Republic)	Lower Devonian (Lochkovian)	E	3	Chlupáč et al. (1980)
A82	1	*Palmatolepis* sp.	Carnic Alps (Italy)	Upper Devonian (Frasnian)	E	4.5	Spalletta & Perri (1998a)
A83	1	*Polygnathus decorosus* Stauffer, 1938	Carnic Alps (Italy)	Upper Devonian (Frasnian)	E	4.5	Spalletta & Perri (1998a)
A80	1	unrecognizable fragment	Carnic Alps (Italy)	Upper Devonian (Famennian)	E	4.5	Perri & Spalletta (1998)
A81	1	*Branmehla werneri* (Ziegler in Flügel & Ziegler, 1957)	Carnic Alps (Italy)	Upper Devonian (Famennian)	E	4.5	Perri & Spalletta (1998)
A101	1	*Palmatolepis triangularis* Sannemann, 1955	Texas (USA)	Upper Devonian (Famennian)	E	2	IPUM Collection
A102	1	*Palmatolepis subperlobata* Branson & Mehl, 1934	Texas (USA)	Upper Devonian (Famennian)	E	2	IPUM Collection
A103	1	*Icriodus* sp.	Texas (USA)	Upper Devonian (Famennian)	E	2	IPUM Collection
S01	1	*Branmehla* sp.	Dzikowiec (Poland)	Upper Devonian (Famennian)	E	3.5	Świś et al. (2026)
S02	1	*Branmehla* sp.	Dzikowiec (Poland)	Upper Devonian (Famennian)	E	3.5	Świś et al. (2026)
S03	1	*Branmehla* sp.	Dzikowiec (Poland)	Upper Devonian (Famennian)	E	3.5	Świś et al. (2026)
S04	1	*Branmehla* sp.	Dzikowiec (Poland)	Upper Devonian (Famennian)	E	3.5	Świś et al. (2026)

Tab. 1 - Continuation.

CODE	N° ELEMENTS	CONODONT TAXA	LOCALITY	SYSTEM/SERIES (STAGE)	P/E	CAI	REFERENCE PAPER(S)/ COLLECTION
S05	1	*Branmehla* sp.	Dzikowiec (Poland)	Upper Devonian (Famennian)	E	3.5	Świś et al. (2026)
S06	1	*Branmehla* sp.	Sardinia (Italy)	Upper Devonian (Famennian)	E	5	Świś et al. (2026)
S07	1	*Branmehla* sp.	Sardinia (Italy)	Upper Devonian (Famennian)	E	5	Świś et al. (2026)
S08	1	*Branmehla* sp.	Sardinia (Italy)	Upper Devonian (Famennian)	E	5	Świś et al. (2026)
S09	1	*Branmehla* sp.	Sardinia (Italy)	Upper Devonian (Famennian)	E	5	Olivieri (1970); Świś et al. (2026)
S010	1	*Bispathodus* sp.	Sardinia (Italy)	Upper Devonian (Famennian)	E	5	Olivieri (1970); Świś et al. (2026)
S011	1	*Bispathodus* sp.	Sardinia (Italy)	Upper Devonian (Famennian)	E	5	Olivieri (1970); Świś et al. (2026)
S012	1	*Bispathodus* sp.	Sardinia (Italy)	Upper Devonian (Famennian)	E	5	Olivieri (1970); Świś et al. (2026)
S013	1	*Bispathodus* sp.	Sardinia (Italy)	Upper Devonian (Famennian)	E	5	Świś et al. (2026)
S014	1	*Bispathodus* sp.	Sardinia (Italy)	Upper Devonian (Famennian)	E	5	Świś et al. (2026)
S015	1	*Palmatolepis* sp.	Kowala (Poland)	Upper Devonian (Famennian)	E	1.5	Świś et al. (2026)
S016	1	*Palmatolepis* sp.	Kowala (Poland)	Upper Devonian (Famennian)	E	1.5	Świś et al. (2026)
S017	1	*Palmatolepis* sp.	Kowala (Poland)	Upper Devonian (Famennian)	E	1.5	Świś et al. (2026)
S018	1	*Palmatolepis* sp.	Kowala (Poland)	Upper Devonian (Famennian)	E	1.5	Świś et al. (2026)
S019	1	*Palmatolepis* sp.	Sardinia (Italy)	Upper Devonian (Famennian)	E	5	Świś et al. (2026)
S020	1	*Palmatolepis* sp.	Sardinia (Italy)	Upper Devonian (Famennian)	E	5	Świś et al. (2026)
S021	1	*Palmatolepis* sp.	Sardinia (Italy)	Upper Devonian (Famennian)	E	5	Świś et al. (2026)
S022	1	*Palmatolepis* sp.	Sardinia (Italy)	Upper Devonian (Famennian)	E	5	Świś et al. (2026)
S023	1	*Palmatolepis* sp.	Sardinia (Italy)	Upper Devonian (Famennian)	E	5	Świś et al. (2026)
A76-A77, A100	3	unrecognizable fragments	Carnic Alps (Italy)	Carboniferous/ Lower Mississippian (Tournaisian)	E	4.5	Spalletta & Perri (1998b)
A78-A79	2	*Gnathodus* sp.	Carnic Alps (Italy)	Carboniferous/ Middle Mississippian (Visean)	E	4-4.5	Spalletta & Perri (1998b)
A86-A87	2	*Pachycladina obliqua* Staesche, 1964	Dolomites (Italy)	Lower Triassic (Olenekian)	E	5.5-6	Perri & Andraghetti (1987)
A84-A85	2	unrecognizable fragments	Dolomites (Italy)	Middle Triassic (Anisian)	E	1.5	Kovács et al. (1996); Farabegoli & Perri (1998)
A42-A43-A44	3	*Carnepigondolella pseudodiebeli* (Kozur, 1972)	Sicily (Italy)	Upper Triassic (Carnian)	E	1.5	Mazza et al. (2012); Mazza & Martínez-Pérez (2015)
Total analyzed conodont elements	126						

Tab. 1 - Continuation.

image-plate detector, a flat graphite monochromator, interchangeable beam collimators, a motorized stage, and a microscope for accurate sample positioning. Measurements were performed in reflection geometry using a 300-μm collimator and a collection time of 30 min. The Omega and Phi angles were adjusted for each sample according to its orientation and the instrumental geometry to maximize the number of detectable diffraction effects and optimize the signal-to-noise ratio. The μ-XRD data were acquired as two-dimensional diffraction images and subsequently converted into 2θ-intensity (2θ-I) profiles using Rigaku R-AXIS Display software. The use of a 300-μm collimator allowed representative mean values of the bioapatite unit-cell parameters to be obtained across the conodont elements as a whole. A subset of euconodont elements was also analyzed at two distinct morphological positions, namely the basal region and the denticle. This within-element comparison was undertaken to investigate possible spatial variations in crystallographic properties and to determine whether the two regions preserve similar or distinct signals. These analyses were performed using a 0.1-mm collimator with a data collection time of 2 hours.

Calculation of Crystallinity Index and $N_{UnitCell}$ parameters

In addition to calculating bioapatite unit-cell parameters (*a* and *c*) and volume using UnitCell (Holland & Redfern, 1997), two independent estimates of sample crystallinity (i.e., the Crystallinity Index and $N_{UnitCell}$) were derived from the μ-XRD data following Medici et al. (2026). To summarize briefly, the first approach involved calculating the Crystallinity Index described by Person et al. (1995), later refined by Pucéat et al. (2004), and modified by Medici et al. (2021) for preferential orientations. The calculation of $N_{UnitCell}$ is based on the Full Width at Half Maximum (FWHM) of the (300) and (002) reflections. More specifically, the Scherrer equation was applied to these reflections to estimate crystallite width along the **a** axis and crystallite length along the **c** axis, respectively (Dumont et al., 2011). The number of coherently diffracting unit-cell repeats (hereafter referred to as "unit cells per crystallite") along the **a**-axis ($N_{UnitCell(a)}$) and **c**-axis ($N_{UnitCell(c)}$) was then estimated from the crystallite width/*a* and length/*c* ratios, respectively.

The CI provides a general measure of the structural organization of bioapatite and has been widely used to assess diagenetic modifications in archeological and paleontological phosphatic tissues. The $N_{UnitCell}$ values, by contrast, express the number of unit cells both along the **a** axis and **c** axis, highlighting any directional differences in crystallite growth.

Statistical analyses were performed to assess the significance of the differences observed among the investigated groups. Group comparisons were conducted using Welch's t-test, with the statistical significance threshold set at $\alpha = 0.05$ ($p < 0.05$ and $p < 0.01$ were considered significant and highly significant, respectively), 95% confidence intervals.

The μ-XRD analyses of the conodonts were influenced by their different morphologies. Although several analyses were performed on each sample, it was not possible to calculate all the parameters for every sample. For this reason, the relationships presented may involve different sample sizes.

RESULTS

The results obtained by μ-XRD reveal distinct crystallographic and crystallinity patterns in paraconodont and euconodont bioapatite. The main unit-cell parameters and crystallinity indices are summarized below. Values are reported as the observed range followed by the mean, with the corresponding standard deviation in parentheses. Importantly, none of the crystallographic parameters analyzed shows any correlation with conodont age. For this reason, the same symbol was used for specimens of different geological ages in the plots. Some elements were analyzed at multiple points; therefore, the number of measurements does not necessarily correspond to the number of individual elements.

Paraconodonts display relatively restricted variations in their unit-cell parameters. The *a* unit-cell parameter ranges from 9.337 to 9.356 Å, with a mean value $\bar{a}$ = 9.348(6) Å, whereas *c* ranges from 6.884 to 6.911 Å, averaging $\bar{c}$ = 6.897(8) Å (Fig. 2a, b). The resulting unit-cell volume (V) varies between 520.5 and 523.6 Å^3, with a mean $\bar{V}$ value of 521.9(1.0) Å^3 (Fig. 2c, d). Crystallinity Index values (Fig. 3a, b) range from 0.360 to 0.682, with a mean value of 0.502(115). The number of coherently diffracting unit cells along the **a** axis, $N_{UnitCell(a)}$, ranges from 31 to 56, with a mean of 41(8), whereas $N_{UnitCell(c)}$ varies between 42 and 75, averaging 63(9) (Fig. 3c-h). The sample sizes for paraconodonts are 11 for unit-cell parameters and 14 for the other crystal parameters.

Euconodonts exhibit broader ranges and generally higher mean values for most of the investigated parameters. The *a* unit-cell parameter ranges from 9.352 to 9.392 Å, with a mean of 9.369(7) Å, whereas the *c* unit-cell parameter varies between 6.857 and 6.907 Å, with a mean of 6.883(8) Å (Fig. 2a, b). Unit-cell volumes range from 520.2 to 525.4 Å^3, averaging 523.3(9) Å^3 (Fig. 2c, d). The sample sizes for the unit-cell parameters of euconodonts are 113. The Crystallinity Index (Fig. 3a, b) shows considerable variability, ranging from 0.256 to 2.105, with a mean of 0.934(0.303) and a sample size of 113. Similarly, $N_{UnitCell(a)}$ values (sample size: 87) range from 63 to 124, with a mean of 90(14), whereas $N_{UnitCell(c)}$ (sample size: 66) ranges from 39 to 162, with a mean of 100(28) (Fig. 3c-h). It should be noted that the paraconodont and euconodont datasets differ substantially in taxonomic composition, stratigraphic coverage, and sample size. Paraconodonts are represented by a limited number of predominantly Cambrian taxa, whereas euconodonts encompass a much broader range of taxa spanning several geological periods. Consequently, the greater dispersion observed in euconodont crystallographic parameters may reflect both differences in biomineralization and the broader biological and temporal diversity represented in the dataset.

The *c* versus *a* unit-cell parameters of the investigated bioapatite samples are plotted in Fig. 2a. Paraconodonts display significantly lower *a* and higher *c* unit-cell parameter values than euconodonts, occupying clearly distinct fields. Welch's *t*-test confirms significant differences between the two groups for both parameters ($p < 0.01$), as well as the Cohen's d and 95% confidence intervals (Cohen's d = -3.05 and 95% confidence interval [-0.026, -0.017] for *a* unit-cell parameter; Cohen's d = 1.74 and 95% confidence interval [0.008, 0.020] for *c*

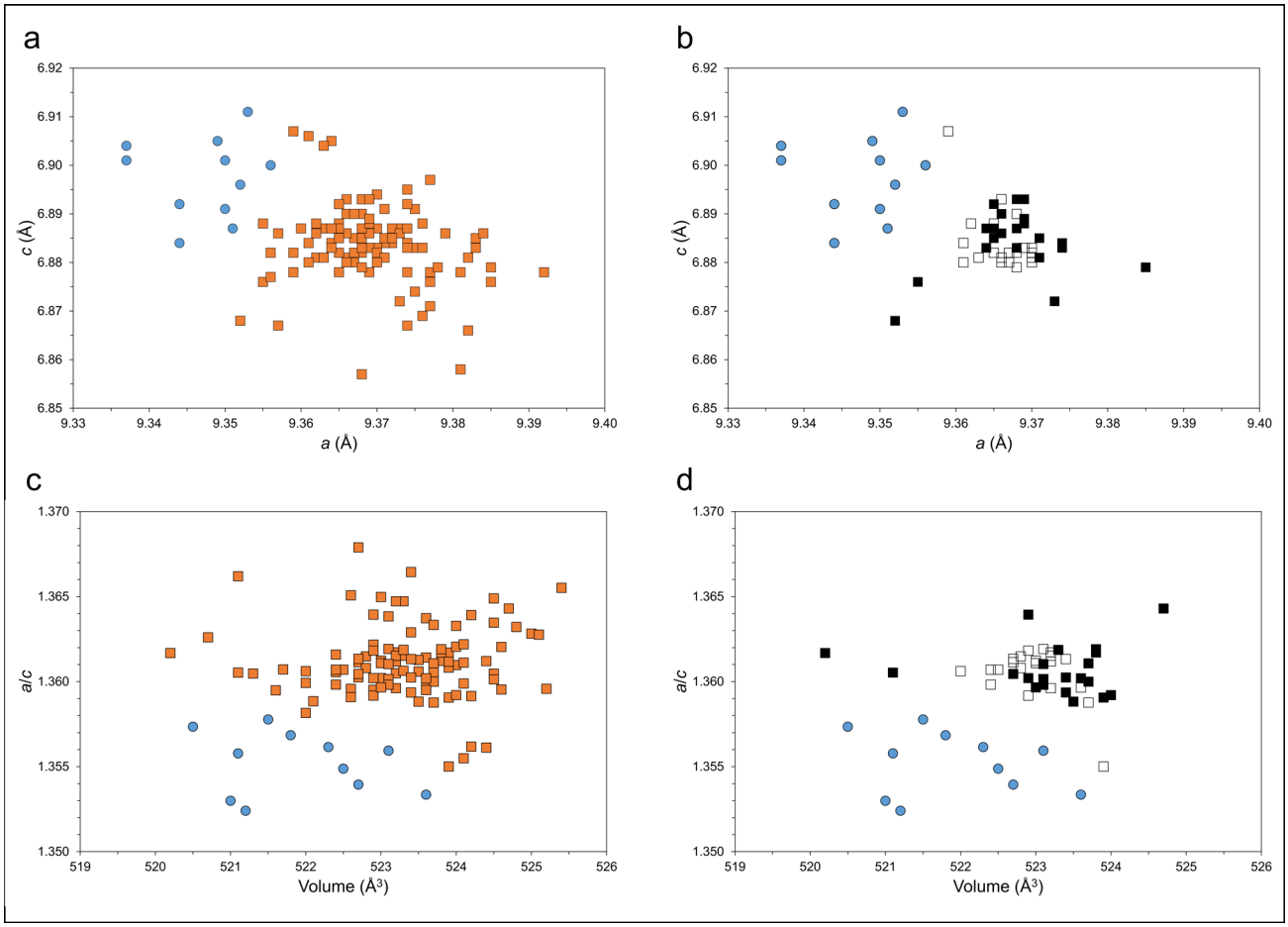

Fig. 2 - (color online) Relationships among bioapatite unit-cell parameters in the investigated conodont elements. a) Plot of the *a* and *c* lattice parameters for paraconodonts (blue circles) and euconodonts (orange squares). b) The same relationship, with euconodont data distinguished between the conodont base (open squares) and denticles (filled squares). c) Relationship between unit-cell volume and the *a*/*c* ratio for paraconodonts and euconodonts. d) The same plot, with the euconodont dataset subdivided as in panel (b). Sample size of paraconodonts: 11 (a, c); sample size of euconodonts: 113 (a, c); sample size of conodont base: 22 (b, d); sample size of conodont denticles: 22 (b, d).

parameter). By contrast, no significant differences in either parameter were observed between the basal and denticle regions of the selected euconodont elements (Fig. 2b; Welch's *t*-test, $p > 0.05$; Cohen's d = -0.393 and 95% confidence interval [-0.005, 0.001] for *a* parameter; Cohen's d = -0.029 and 95% confidence interval [-0.004, 0.004] for *c* parameter). Similar patterns are observed for unit-cell volume and the *a*/*c* ratio (Fig. 2c, d), with statistically significant differences between paraconodonts and euconodonts (Welch's *t*-test, $p < 0.01$; Cohen's d = -1.49 and 95% confidence interval [-2.05, -0.70] for unit-cell volume; Cohen's d = -2.87 and 95% confidence interval [-0.007, -0.005] for *a*/*c* ratio). Figure 3a shows the CI values and highlights the distinct pattern displayed by paraconodonts (Welch's *t*-test, $p < 0.01$; Cohen's d = -1.49; 95% confidence interval [-0.517, -0.348]). Their low CI values support the hypothesis of a higher carbonate content compared with euconodonts (Person et al., 1995). Figure 3b shows no clear distinction between CI values from the basal and denticle regions of euconodont elements (Welch's *t*-test, $p > 0.05$; Cohen's d = -0.535; 95% confidence interval [-0.418, 0.029]).

$N_{UnitCell(a)}$ and $N_{UnitCell(c)}$ are crystallinity parameters that normalize crystallite dimensions along the **a** and **c** axes using the corresponding unit-cell parameters, thereby expressing the number of unit cells within the crystallites along each crystallographic direction. $N_{UnitCell(a)}$ reveals a clear difference between paraconodonts and euconodonts (Fig. 3d, f) (Welch's *t*-test, $p < 0.01$; Cohen's d = -3.54; 95% confidence interval [-54.2, -43.4]). Paraconodonts display a lower number of unit cells along the **a** axis, consistent with their lower CI values (Fig. 3f).

Fig. 3 - (color online) Relationships among bioapatite unit-cell volume, Crystallinity Index (CI), and crystallite dimensions in paraconodonts and euconodonts. a) Relationship between unit-cell volume and CI for paraconodonts (blue circles) and euconodonts (orange squares). b) The same relationship, with euconodont data distinguished between data collected from the conodont base (open squares) and denticles (filled squares). c, d) Relationships between unit-cell volume and the number of unit cells per crystallite along the **c** and **a** axes, respectively. e, f) Relationships between CI and the number of unit cells per crystallite along the **c** and **a** axes, respectively. (g) Relationship between the number of unit cells per crystallite along the **a** and **c** axes; the dashed line represents the 1:1 relationship. h) The same relationship for the subset of euconodont data distinguished as in panel (b). Sample size of paraconodonts: 14; sample size of euconodonts: 113 (a), 66 (c, e), 87 (d, f), 63 (g); sample size of conodont base: 23 (b), 16 (h); sample size of conodont denticles: 22 (b), 11 (h).

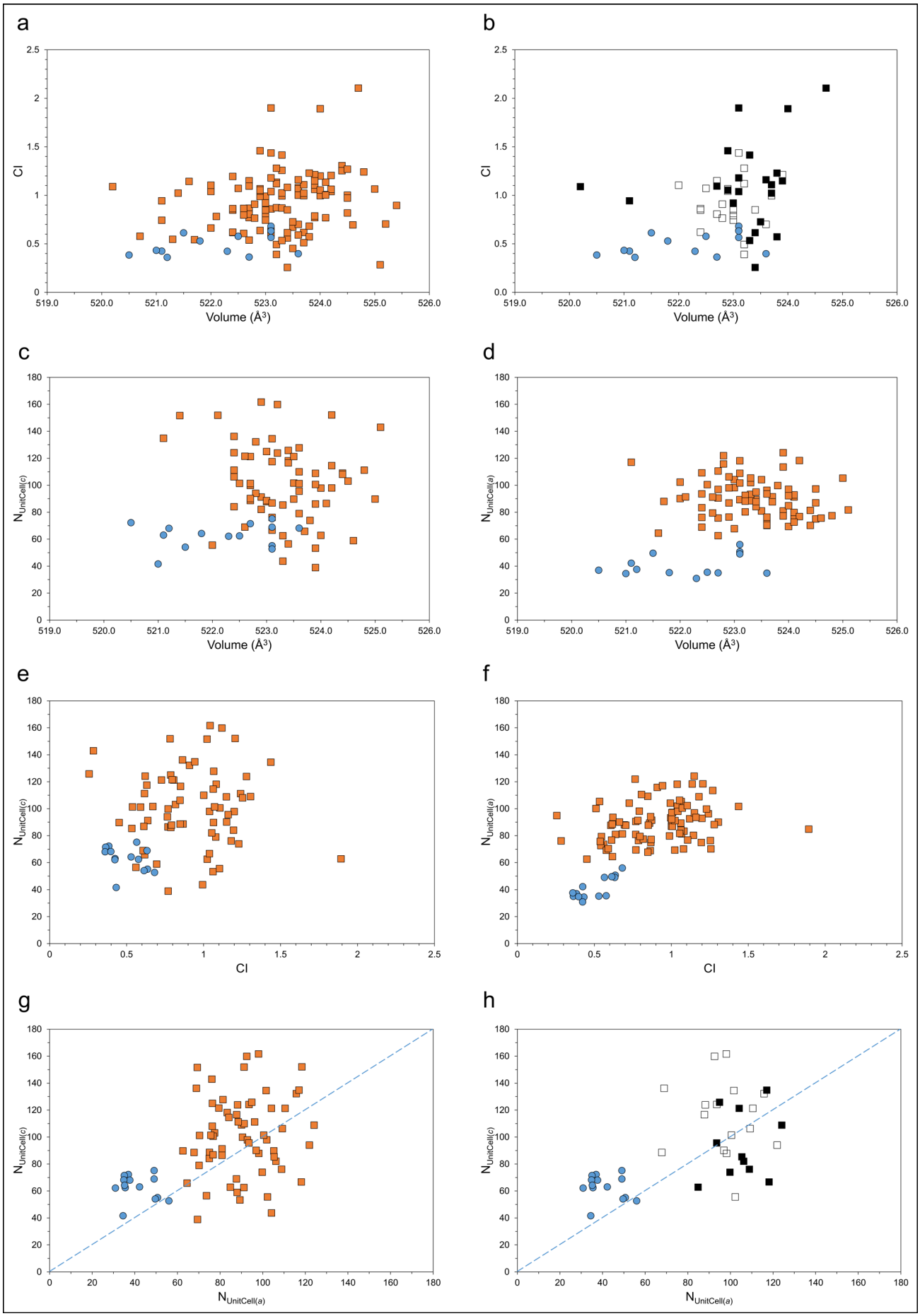
a
CI
Volume (Å³)
b
CI
Volume (Å³)
c
N UnitCell(c)
Volume (Å³)
d
N UnitCell(a)
Volume (Å³)
e
N UnitCell(c)
CI
f
N UnitCell(a)
CI
g
N UnitCell(c)
N UnitCell(a)
h
N UnitCell(c)
N UnitCell(a)

$N_{UnitCell(c)}$ values show a less clear relationship with CI and unit-cell volume (Fig. 3c, e), owing to the partial overlap between paraconodont and euconodont values. Nevertheless, paraconodonts generally exhibit a low number of unit cells along the **c** axis. Statistical analysis confirms a significant difference in $N_{UnitCell(c)}$ between paraconodonts and euconodonts (Welch's *t*-test, $p < 0.01$; Cohen's d = -1.46; 95% confidence interval [-45.9, -29.1]).

Figure 3g compares the number of coherently diffracting unit-cell repeats along the two crystallographic directions. Paraconodonts show significantly higher $N_{UnitCell(c)}$ than $N_{UnitCell(a)}$ values. Euconodonts show a less distinct pattern, although statistical analysis indicates slightly preferential growth along the **c** axis (Welch's *t*-test, $0.01 < p < 0.05$; Cohen's d = 0.487; 95% confidence interval [2.88, 17.8]). Figure 3h and the corresponding statistical analysis show no clear differences between the basal (sample size: 16) and denticle (sample size: 11) regions of the selected euconodont elements (Welch's *t*-test, $p > 0.05$, Cohen's d = 0.769 and 95% confidence interval [-0.656, 42.0] for $N_{UnitCell(c)}$; Welch's *t*-test, $p > 0.05$, Cohen's d = -0.596 and 95% confidence interval [-18.5, 2.42] for $N_{UnitCell(a)}$). However, slight differences appear to emerge within the basal group, for which the statistical analysis suggests higher $N_{UnitCell(c)}$ than $N_{UnitCell(a)}$ values (Welch's *t*-test, $0.01 < p < 0.05$, Cohen's d = 0.783; 95% confidence interval [1.11, 33.9]). In contrast, the denticle group does not show the same trend (Welch's *t*-test, $p > 0.05$, Cohen's d = -0.574; 95% confidence interval [-29.2, 6.67]). These results should be further investigated using larger sample sizes.

Figure 4 compares the results obtained for conodonts with those for fossil and extant sharks, in which root and crown tissues were analyzed separately (Medici et al., 2026). Many conodont values fall outside the fields defined by shark tissues, although some areas of overlap occur. In Fig. 4a, paraconodont unit-cell parameters only partially overlap the field of fossil shark roots, mainly because of the high *c* values recorded in paraconodonts. Euconodonts show the greatest overlap with fossil shark crowns, a more limited overlap with extant shark roots, and an even smaller overlap with extant shark crowns.

Figure 4b shows limited overlap between paraconodonts and fossil shark roots because of the higher unit-cell volumes of paraconodonts, whereas their CI values are comparable. Euconodonts partially overlap the fossil shark crown field, while their overlap with extant shark crowns is limited and that with extant shark roots is negligible.

Figure 4c confirms the partial overlap between paraconodonts and fossil shark roots, both of which exhibit preferential crystallite growth along the **c** axis. Euconodonts show considerable overlap with the crown tissues of both fossil and extant sharks, whereas their overlap with extant shark roots is limited.

DISCUSSION

The results discussed above reflect the distinctive characteristics of paraconodonts, whose inferred high carbonate content is consistent with lower *a* and higher *c* unit-cell parameter values (Cacciotti, 2016). Their low crystallinity indices further distinguish paraconodonts from euconodonts.

From an experimental perspective, it should be noted that analysis of the (002) reflection, used to calculate $N_{UnitCell(c)}$, is more challenging than that of the (300) reflection, used to calculate $N_{UnitCell(a)}$. In some euconodonts, such as *Scabbardella altipes*, element morphology combined with the experimental geometry of the microdiffractometer makes the (002) reflection difficult to detect. Consequently, some of the data points reported in Fig. 3c, e, g may be less accurate.

Importantly, the relative numbers of unit-cell repeats must be distinguished from the physical dimensions of the coherent domains. Based on the group mean values, paraconodont domains are 39(8) nm along the **a** axis and 43(6) nm along the **c** axis, whereas euconodont domains are 84(14) nm along the **a** axis and 69(19) nm along the **c** axis. Given the low statistical significance of the differences in crystallite width and length, the $N_{UnitCell}$ parameter is necessary to better understand the preferential growth along the two crystallographic directions both in paraconodonts and euconodonts.

Despite the partial overlap observed between paraconodonts and fossil shark roots in some of the investigated parameters, any inference concerning their original organic content remains highly tentative. Shark roots originally contained a higher proportion of organic matter than crown tissues. The crystallographic similarities observed here may therefore suggest that paraconodont elements also contained more organic matter than euconodont elements. If confirmed by independent evidence, this difference could reflect changes in tissue organization and biomineralization during the evolutionary transition from paraconodonts to euconodonts. However, a direct relationship between organic content, feeding efficiency, and crystallographic properties cannot be established from the present data alone and remains a hypothesis requiring further investigation.

As discussed earlier, paraconodonts occupy a relatively restricted field characterized by generally smaller crystallite dimensions for both the (002) and (300) reflections, whereas euconodonts exhibit larger values and substantially greater variability. This pattern suggests that the transition from paraconodont to euconodont mineralized tissues was associated with a change in the size and/or organization of apatite crystallites. The distinction appears particularly pronounced for the

Fig. 4 - (color online) Comparison of the crystallographic properties of paraconodont and euconodont bioapatite with those reported for crown and root tissues of fossil and extant shark teeth. a) Distribution of the *a* and *c* unit-cell parameters. b) Relationship between unit-cell volume and Crystallinity Index (CI). c) Relationship between the number of unit cells per crystallite along the **a** and **c** axes; the dashed line represents the 1:1 relationship. Paraconodonts are indicated by blue circles and euconodonts by orange squares. Colored fields delimit the ranges reported for fossil shark roots (yellow), fossil shark crowns (light blue), extant shark roots (red), and extant shark crowns (green). These fields are manually drawn outlines encompassing the overall spread of values reported by Medici et al. (2026) for each shark tissue group and are included solely as qualitative visual references. They do not represent statistical confidence regions or density estimates. Their boundaries may be influenced by extreme values, and overlap with conodont data is interpreted descriptively.

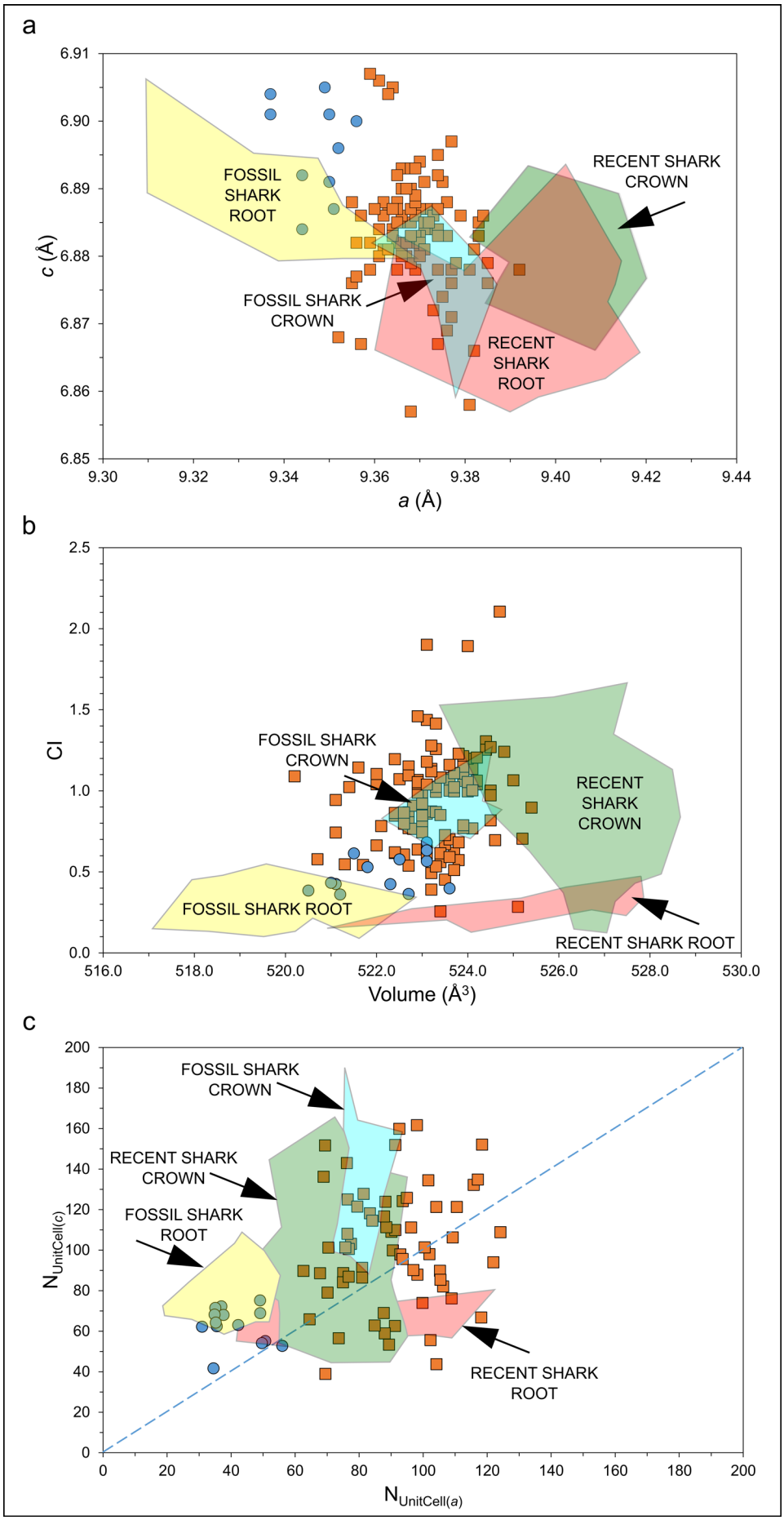
a
6.91
6.90
6.89
6.88
6.87
6.86
6.85
c (Å)
9.30
9.32
9.34
9.36
9.38
9.40
9.42
9.44
a (Å)
FOSSIL SHARK ROOT
RECENT SHARK CROWN
FOSSIL SHARK CROWN
RECENT SHARK ROOT
b
2.5
2.0
1.5
1.0
0.5
0.0
CI
516.0
518.0
520.0
522.0
524.0
526.0
528.0
530.0
Volume (Å3)
FOSSIL SHARK CROWN
RECENT SHARK CROWN
FOSSIL SHARK ROOT
RECENT SHARK ROOT
c
200
180
160
140
120
100
80
60
40
20
0
N UnitCell(c)
0
20
40
60
80
100
120
140
160
180
200
N UnitCell(a)
FOSSIL SHARK CROWN
RECENT SHARK CROWN
FOSSIL SHARK ROOT
RECENT SHARK ROOT

(300) crystallite dimension, which may indicate that the evolutionary differentiation of euconodont tissues involved preferential changes in crystal dimensions along specific crystallographic directions rather than a uniform increase in crystallite size. The relationship between (300) and (002) crystallite dimensions is especially informative in this respect. The two parameters do not appear to increase proportionally, and there is no clear correlation within either paraconodonts or euconodonts considered as a whole (sample size: 14, Pearson's $r = -0.16$, p-value = 0.583, and sample size: 63, Pearson's $r = 0.15$ and p-value = 0.244, respectively). Thus, the larger crystallites observed in euconodonts should not be interpreted simply as the result of isotropic crystal growth. Instead, the data are more consistent with a change in the anisotropy and structural organization of the apatite crystallites. In other words, the transition to the euconodonts may have involved not only an increase in crystallite dimensions, but also a modification of how crystal growth was controlled along different crystallographic axes.

The relationship between crystallite dimensions and the CI provides an additional indication that crystallinity evolved in a more complex manner than a simple increase in crystal size. Among paraconodonts, the CI is strongly positively correlated with the (300) crystallite dimension (sample size: 14, $r = 0.80$, p-value = $6.24 \cdot 10^{-4}$), whereas a comparable relationship is not evident for the (002) dimension (sample size: 14, $r = -0.32$, p-value = 0.270). In euconodonts, however, this relationship is substantially weaker when the samples are considered together. This suggests that CI cannot be regarded as a straightforward proxy for crystallite size across all conodont mineralized tissues. Instead, the relationship between crystallinity and crystallite dimensions appears to be tissue-dependent, potentially reflecting differences in crystal organization, orientation, or other aspects of mineral microstructure associated with the differentiation of euconodont tissues.

Similarly, the plots involving unit-cell volume do not reveal a single, continuous relationship shared by paraconodonts and euconodonts. The broader dispersion of euconodont values, together with the different behavior of the individual groups, argues against interpreting the crystallographic changes as a simple linear trajectory from a paraconodont to a euconodont condition. Rather, the data suggest that the emergence of euconodont mineralized tissues was accompanied by a reorganization of apatite crystallography, followed by further diversification potentially associated with tissue differentiation.

The broader dispersion of euconodont values, however, cannot be attributed solely to tissue differentiation. The paraconodont and euconodont datasets also differ in age, taxonomic composition, geographic provenance, abundance, and diagenetic history, and the within-element comparisons between basal and denticle regions do not reveal significant differences. Moreover, the μ-XRD beam may integrate more than one microstructural domain. The observed group-level patterns are therefore consistent with crystallographic reorganization during the paraconodont-euconodont transition, but their biological component cannot yet be fully separated from taxonomic, preservational, and analytical variability.

No clear systematic relationship between CAI and CI was observed in the investigated dataset. Similarly, Zhang et al. (2017) reported no relationship between CAI and the other parameters analyzed, despite documenting diagenetic recrystallization in conodont apatite. Medici et al. (2021) further showed that relationships between CI and geochemical indicators of alteration depend on the method used to calculate crystallinity. These findings emphasize that crystallinity and thermal maturity need not vary together. Accordingly, the CAI-CI comparison provides only a partial assessment of diagenetic influences, and the absence of a systematic relationship cannot establish an exclusively biological origin for the observed crystallographic differences.

From an evolutionary perspective, these results are particularly interesting when considered alongside the model proposed by Murdock et al. (2013, 2014). The transition from paraconodonts to euconodonts has been interpreted as a stepwise acquisition of tissue differentiation, culminating in the development of a distinct crown and basal body. The crystallographic data appear compatible with this scenario, because euconodonts do not simply extend the paraconodont range toward higher crystallinity. Instead, the crystallographic data indicate that they occupy a broader and partly distinct region of crystallographic parameter space, consistent with the possibility that the acquisition of differentiated tissues was accompanied by changes in the organization of the mineral phase. Murdock et al. (2014) similarly emphasized that differentiation of the euconodont crown produced important changes in the mechanical behavior of the element, particularly by increasing stiffness and reducing strain under loading. The crystallographic differences observed here could therefore provide an additional level of evidence for the progressive structural specialization of conodont mineralized tissues, although a direct causal relationship between crystallographic parameters and mechanical properties cannot be established from these data alone.

Nevertheless, the combination of larger and more variable crystallite dimensions, anisotropic changes between the (002) and (300) directions, and the altered relationship between crystallite size and CI suggests that the origin and subsequent differentiation of euconodont tissues involved a substantial reorganization of apatite at the crystallographic level.

Taken together, these data indicate that the transition from paraconodont to euconodont mineralized tissues was associated with a marked change in crystallite dimensions and organization. Euconodonts generally exhibit larger crystallite dimensions and greater variability than paraconodonts, with the distinction being particularly evident for the (300) reflection. However, the absence of a consistent correlation between (002) and (300) crystallite dimensions suggests that this transition did not involve simple isotropic crystal growth, but rather a modification of crystallite anisotropy and organization. The relationship between crystallite dimensions and CI is likewise tissue-dependent: in paraconodonts, CI is strongly associated with the (300) crystallite dimension, whereas this relationship is largely absent when euconodonts are considered as a whole. Together with the lack of a simple relationship with unit-cell volume, these results suggest that euconodont tissue differentiation involved a reorganization of the apatite mineral phase rather than merely an increase in

crystallinity. This pattern is consistent with the stepwise evolutionary differentiation of euconodont mineralized tissues proposed by Murdock et al. (2013) and with the subsequent functional specialization of the crown demonstrated by Murdock et al. (2014).

CONCLUSION

This study provides new crystal-chemical evidence for clear group-level differences between paraconodont and euconodont bioapatite. The integration of unit-cell parameters, crystallite dimensions and Crystallinity Index demonstrates that paraconodonts occupy a comparatively restricted crystallographic field, whereas euconodonts are characterized by larger crystallite dimensions and a substantially greater variability. The recurrence of these group-level differences across a geographically and stratigraphically broad dataset is consistent with a retained biological component, although variation in age, provenance, taxonomic composition, and diagenetic history may also contribute to the observed distributions.

The inferred higher carbonate content of paraconodont bioapatite remains a hypothesis based on unit-cell parameters. A concrete next step would be to compare carbonate contents in paraconodont and euconodont apatite using appropriately calibrated FTIR measurements targeting lattice-bound carbonate, thereby independently testing the proposed compositional difference.

The relationships among crystallite dimensions, Crystallinity Index and unit-cell volume further indicate that the paraconodont-euconodont transition cannot be interpreted simply as an increase in apatite crystallinity. Rather, the data point to a more complex reorganization of the mineral phase, involving changes in crystallite size, anisotropy and structural organization.

These crystal-chemical differences complement the previously recognized histological distinction between the comparatively simple mineralized tissues of paraconodonts and the differentiated crown and basal body of euconodonts. They are therefore consistent with a stepwise transition toward increasingly differentiated conodont hard tissues and suggest that this evolutionary transformation involved changes in mineral organization at the crystallographic scale. More broadly, the paraconodont-euconodont contrast partly parallels crystallographic differences between root and crown tissues in sharks, providing a comparative framework, rather than evidence of tissue homology, for investigating early vertebrate biomineralization.

ACKNOWLEDGEMENTS

We are deeply grateful to the many colleagues who generously provided conodont material included in this study and contributed their expertise to the taxonomic identification and assignment of the specimens. Their willingness to share material, knowledge, and expertise was invaluable to the development of the dataset analyzed herein. We are also grateful to Guillermo Albanesi and Carlo Corradini, as well as to BSPI Co-Editor Johannes Pignatti, for their insightful and constructive comments, which greatly improved the clarity, focus, and overall quality of the manuscript.

This paper is a contribution to IGCP Project n. 735 “Rocks and the Rise of Ordovician Life: Filling knowledge gaps in the Early Palaeozoic Biodiversification.”

REFERENCES

Aldridge R.J., Purnell M.A., Gabbott S.E. & Theron J.N. (1995). The apparatus architecture and function of *Promissum pulchrum* Kovács-Endrödy (Conodonta, Upper Ordovician) and the prioniodontid plan. *Philosophical Transactions of the Royal Society of London, Series B, Biological Sciences*, 347: 275-291.

Bagnoli G., Ferretti A., Serpagli E. & Vai G.B. (1998). Late Ordovician conodonts from the Valbertad section (Carnic Alps). *Giornale di Geologia*, 60: 138-149.

Bengtson S. (1976). The structure of some Middle Cambrian conodonts, and the early evolution of conodont structure and function. *Lethaia*, 9: 185-206.

Bengtson S. (1983). The early history of the conodonta. *Fossils and Strata*, 15: 5-19.

Bergström S.M. & Ferretti A. (2015). Conodonts in the Upper Ordovician Keisley Limestone of northern England: taxonomy, biostratigraphical significance and biogeographical relationships. *Papers in Palaeontology*, 1: 1-32.

Bischoff G. & Sannemann D. (1958). Unterdevonische Conodonten aus dem Frankenwald. *Notizblatt des Hessischen Landesamtes für Bodenforschung zu Wiesbaden*, 86: 87-110.

Branson E.B. & Mehl M.G. (1933). Conodonts from the Maquoketa Thebes (Upper Ordovician) of Missouri. *University of Missouri Studies*, 8: 121-132.

Branson E.B. & Mehl M.G. (1934). Conodonts from the Grassy Creek Shale of Missouri. *University of Missouri Studies*, 8: 171-259.

Branson E.B., Mehl M.G. & Branson C.C. (1951). Richmond Conodonts of Kentucky and Indiana. *Journal of Paleontology*, 25: 1-17.

Cacciotti I. (2016). Cationic and anionic substitutions in hydroxyapatite. *In* Antoniac I.V. (ed.), Handbook of Bioceramics and Biocomposites. Springer, Cham: 145-211.

Chlupáč I., Kříž J. & Schönlaub H.P. (1980). Field trip E, ECOS II, Barrandian. *Abhandlungen der Geologischen Bundesanstalt*, 35: 147-180.

Corradini C., Ferretti A. & Serpagli E. (1998). The Silurian and Devonian sequence in SE Sardinia. *Giornale di Geologia*, 60: 71-74.

Corradini C., Henderson C., Barrick J.E. & Ferretti A. (2026). Conodonts in Biostratigraphy. A 300-million-years long journey through geologic time. *Newsletters on Stratigraphy*, 59: 77-116.

Donoghue P.C.J. (1998). Growth and patterning in the conodont skeleton. *Philosophical Transactions of the Royal Society of London, Series B, Biological Sciences*, 353: 633-666.

Du Y., Chiari M., Karádi V., Nicora A., Onoue T., Pálfy J., Roghi G., Tomimatsu Y. & Rigo M. (2020). The asynchronous disappearance of conodonts: new constraints from Triassic-Jurassic boundary sections in the Tethys and Panthalassa. *Earth-Science Reviews*, 203: 103176.

Du Y., Onoue T., Tomimatsu Y., Wu Q. & Rigo M. (2023). Lower Jurassic conodonts from the Inuyama area of Japan: implications for conodont extinction. *Frontiers in Ecology and Evolution*, 11: 1135789.

Dumont M., Kostka A., Sander P.M., Borbely A. & Kaysser-Pyzalla A. (2011). Size and size distribution of apatite crystals in sauropod fossil bones. *Palaeogeography, Palaeoclimatology, Palaeoecology*, 310: 108-116.

Farabegoli E. & Perri M.C. (1998). Scythian and Anisian conodonts from the Sotto le Rive section (Southern Alps, Italy). *Giornale di Geologia*, 60: 254-259.

Ferretti A. & Serpagli E. (1999). Late Ordovician conodont faunas from southern Sardinia, Italy: biostratigraphic and paleogeographic implications. *Bollettino della Società Paleontologica Italiana*, 37: 215-236.

Ferretti A., Messori A. & Bergström S.M. (2014a). Composition and significance of the Katian (Upper Ordovician) conodont fauna of the Vaux Limestone ("Calcaire des Vaux") in Normandy, France. *Estonian Journal of Earth Sciences*, 63: 214-219.

Ferretti A., Bergström S.M. & Sevastopulo G.D. (2014b). Katian conodonts from the Portrane limestone: The first Ordovician conodont fauna described from Ireland. *Bollettino della Società Paleontologica Italiana*, 53: 105-119.

Ferretti A., Malferrari D., Medici L. & Savioli M. (2017). Diagenesis does not invent anything new: precise replication of conodont structures by secondary apatite. *Scientific Reports*, 7: 1624.

Ferretti A., Bancroft A.M. & Repetski J.E. (2020). GECkO: Global events impacting COnodont evolution. *Palaeogeography, Palaeoclimatology, Palaeoecology*, 549: 109677.

Ferretti A., Medici L., Savioli M., Mascia M.T. & Malferrari D. (2021). Dead, fossil or alive: Bioapatite diagenesis and fossilization. *Palaeogeography, Palaeoclimatology, Palaeoecology*, 579: 110608.

Ferretti A., Corradini C., Fakir S., Malferrari D. & Medici L. (2023). To be or not to be a conodont. The controversial story of *Pseudooneotodus* and *Eurytholia*. *Marine Micropaleontology*, 182: 102258.

Ferretti A., Bergström S.M. & Spalletta C. (2025). A Late Ordovician conodont fauna from the Uqua Section, Carnic Alps, Italy. *Bollettino della Società Paleontologica Italiana*, 64: 395-407.

Flügel H. & Ziegler W. (1957). Die Gliederung des Oberdevons und Unterkarbons am Steinberg westlich von Graz mit Conodonten. *Mitteilungen des naturwissenschaftlichen Vereins für Steiermark*, 87: 25-60.

Haridy Y., Norris S.C.P., Fabbri M., Nanglu K., Sharma N., Miller J.F., Rivers M., La Riviere P., Vargas P., Ortega-Hernández J. & Shubin N.H. (2025). The origin of vertebrate teeth and evolution of sensory exoskeletons. *Nature*, 642: 119-124.

Henningsmoen G. (1948). The *Tretaspis* Series of the Kullatorp Core. *Bulletin of the Geological Institution of the University of Uppsala*, 32: 374-432.

Holland T.J.B. & Redfern S.A.T. (1997). Unit cell refinement from powder diffraction data: the use of regression diagnostics. *Mineralogical Magazine*, 61: 65-77.

Knüpfer J. (1967). Zur Fauna und Biostratigraphie des Ordoviziums (Gräfenthaler Schichten) in Thüringen. *Freiberger Forschungshefte*, C220: 1-119.

Kovács S., Papšová S. & Perri M.C. (1996). New Middle Triassic conodonts of the *Gondolella szabòi-G. trammeri* lineage from the West Carpathian Mts and from the Southern Alps. *Acta Geologica Hungarica*, 39: 101-128.

Kozur H. (1972). Die Conodontengattung *Metapolygnathus* Hayashi, 1968 und ihr stratigraphischer Wert. *Geologisch-Paläontologische Mitteilungen Innsbruck*, 2: 1-37.

Lindström M. (1955). Conodonts from the lowermost Ordovician strata in south-central Sweden. *Geologiska Föreningens i Stockholm Förhandlingar*, 76: 517-604.

Liu H.P., Bergström S.M., Witzke B.J., Briggs D.E.G., McKay R.M. & Ferretti A. (2017). Exceptionally preserved conodont apparatuses with giant elements from the Middle Ordovician Winneshiek Konservat-Lagerstätte, Iowa, USA. *Journal of Paleontology*, 91: 493-511.

Malferrari D., Ferretti A., Mascia M.T., Savioli M. & Medici L. (2019). How much can we trust major element quantification in bioapatite investigation? *ACS Omega*, 4: 17814-17822.

Malferrari D., Ferretti A. & Medici L. (2024). The origin and significance of euhedral apatite crystals on conodonts. *Marine Micropaleontology*, 186: 102308.

Mazza M. & Martínez-Pérez C. (2015). Unravelling conodont (Conodonta) ontogenetic processes in the Late Triassic through growth series reconstructions and X-ray microtomography. *Bollettino della Società Paleontologica Italiana*, 54: 161-186.

Mazza M., Rigo M. & Gullo M. (2012). Taxonomy and stratigraphic record of the Upper Triassic conodonts of the Pizzo Mondello section (Western Sicily, Italy), GSSP candidate for the base of the Norian. *Rivista Italiana di Paleontologia e Stratigrafia*, 118: 85-130.

Medici L., Malferrari D., Savioli M. & Ferretti A. (2020). Mineralogy and crystallization patterns in conodont bioapatite from first occurrence (Cambrian) to extinction (end-Triassic). *Palaeogeography, Palaeoclimatology, Palaeoecology*, 549: 109098.

Medici L., Savioli M., Ferretti A. & Malferrari D. (2021). Zooming in REE and other trace elements on conodonts: Does taxonomy guide diagenesis? *Journal of Earth Science*, 32: 501-511.

Medici L., Ferretti A., Collareta A., Bosio G., Bianucci G., Carnevale G., Casati S., Clò S., Lanteri L., Lugli F., Marramà G., Mollen F.H., Savioli M. & Malferrari D. (2026). Bioapatite crystallinity and Rare Earth Element signatures in fossil and Recent sharks: A window into Past and Present seas. *Chemical Geology*, 702: 123200.

Michailow M.M., Lugli F., Cipriani A., Della Giustina F., Ferretti A., Malferrari D., Fowler D., Freedman Fowler E., Weber M. & Tütken T. (2025). Combined Ca, Sr isotope and trace element analyses of Late Cretaceous dinosaur teeth: assessing diet *versus* diagenesis. *Geochimica et Cosmochimica Acta*, 400: 172-189.

Müller K.J. (1962). Supplement to systematics of conodonts. *In* Moore R.C. (ed.), Treatise on Invertebrate Paleontology, W, Miscellanea. Geological Society of America, Boulder, Colorado, and University of Kansas Press, Lawrence, Kansas: W246-W249.

Müller K.J. & Hinz I. (1991). Upper Cambrian conodonts from Sweden. *Fossils and Strata*, 28: 1-153.

Müller K.J. & Nogami Y. (1971). Über den Feinbau der Conodonten. *Memoirs of the Faculty of Science, Kyoto University, Series of Geology and Mineralogy*, 38: 1-87.

Müller K.J. & Nogami Y. (1972). Growth and function of conodonts. 24th International Geological Congress, Montreal, Section 7: 20-27.

Murdock D.J.E., Dong X.-P., Repetski J.E., Marone F., Stampanoni M. & Donoghue P.C.J. (2013). The origin of conodonts and of vertebrate mineralized skeletons. *Nature*, 502: 546-549.

Murdock D.J.E., Rayfield E.J. & Donoghue P.C.J. (2014). Functional adaptation underpinned the evolutionary assembly of the earliest vertebrate skeleton. *Evolution & Development*, 16: 354-361.

Murphy M.A. & Valenzuela-Ríos J.I. (1999). *Lanea* new genus, lineage of Early Devonian conodonts. *Bollettino della Società Paleontologica Italiana*, 37: 321-334.

Olivieri R. (1970). Conodonti e zonatura del Devoniano superiore e riconoscimento del Carbonifero inferiore nei calcari di Corona Mizziu (Gerrei Sardegna). *Bollettino della Società Paleontologica Italiana*, 8: 63-152.

Perri M.C. & Andraghetti M. (1987). Permian–Triassic boundary and Early Triassic conodonts from the Southern Alps, Italy. *Rivista Italiana di Paleontologia e Stratigrafia*, 93: 291-328.

Perri M.C. & Spalletta C. (1998). Latest Devonian and Early Carboniferous conodonts from the Casera Collinetta di Sotto A section (Carnic Alps, Italy). *Giornale di Geologia*, 60: 168-181.

Person A., Bocherens H., Saliège J.-F., Paris F., Zeitoun V. & Gérard M. (1995). Early diagenetic evolution of bone phosphate: An X-Ray diffractometry analysis. *Journal of Archaeological Science*, 22: 211-221.

Pietzner H., Vahl J., Werner H. & Ziegler W. (1968). Zur chemischen Zusammensetzung und Mikromorphologie der Conodonten. *Palaeontographica Abteilung A*, 128: 115-152.

Pucéat E., Reynard B. & Lécuyer C. (2004). Can crystallinity be used to determine the degree of chemical alteration of biogenic apatites? *Chemical Geology*, 205: 83-97.

Purnell M.A., Donoghue P.C.J. & Aldridge R.J. (2000). Orientation and anatomical notation in conodonts. *Journal of Paleontology*, 74: 113-122.

Reeves J.C., Wogelius R.A., Edwards N.P., Manning P.L. & Sansom R.S. (2026). Early vertebrate biomineralization and eye structure determined by synchrotron X-ray analyses of Silurian jawless fish. *Proceedings of the Royal Society B*, 293: 20252248.

Sannemann D. (1955). Beitrag zur Untergliederung des Oberdevons nach Conodonten. *Neues Jahrbuch für Geologie und Paläontologie, Abhandlungen*, 100: 324-331.

Sansom I.J. (1996). *Pseudooneotodus*: a histological study of an Ordovician to Devonian vertebrate lineage. *Zoological Journal of the Linnean Society*, 118: 47-57.

Sansom I.J., Smith M.P. & Smith M.M. (1994). Dentine in conodonts. *Nature*, 368: 591.

Schönlaub H.P., Corradini C., Corriga M.G. & Ferretti A. (2017). Chrono-, litho- and conodont bio-stratigraphy of the Rauchkofel Boden Section (Upper Ordovician-Lower Devonian), Carnic Alps, Austria. *Newsletters on Stratigraphy*, 50: 445-469.

Spalletta C. & Perri M.C. (1998a). The Frasnian-Famennian boundary at the Pramosio A section (Carnic Alps, Italy). *Giornale di Geologia*, 60: 198-205.

Spalletta C. & Perri M.C. (1998b). Lower Carboniferous conodonts at the Tournaisian/Visean boundary in the Dolina section (Carnic Alps, Italy). *Giornale di Geologia*, 60: 244-253.

Staesche U. (1964). Conodonten aus dem Skyth von Südtirol. *Neues Jahrbuch für Geologie und Paläontologie, Abhandlungen*, 119: 247-306.

Stauffer C.R. (1938). Conodonts of the Olentangy Shale. *Journal of Paleontology*, 12: 411-443.

Świś P.L., Ferretti A., Rigo M., Letulle T., Lugli F., Medici L. & Malferrari D. (2026). Integrated crystallographical indicators and REE–HFSE geochemistry in conodont apatite: evidence for decoupled diagenetic signals. *Marine Micropaleontology*, 207: 102618.

Szaniawski H. (1971). New species of Upper Cambrian conodonts from Poland. *Acta Palaeontologica Polonica*, 16: 401-413.

Szaniawski H. (1982). Chaetognath grasping spines recognized among Cambrian protoconodonts. *Journal of Paleontology*, 56: 806-810.

Trueman C.N., Privat K. & Field J. (2008). Why do crystallinity values fail to predict the extent of diagenetic alteration of bone mineral? *Palaeogeography, Palaeoclimatology, Palaeoecology*, 266: 160-167.

Viira V. (1970). Conodonts of the Varangu Member (Estonian Upper Tremadoc). *Eesti NSV Teaduste Akadeemia Toimetised, Keemia Geoloogia*, 19: 224-233. [in Russian]

Walliser O.H. (1964). Conodonten des Silurs. *Abhandlungen des Hessischen Landesamtes für Bodenforschung,* 41: 1-106.

Zhang L., Cao L., Zhao L., Algeo T.J., Chen Z.-Q., Li Z., Lv Z. & Wang X. (2017). Raman spectral, elemental, crystallinity, and oxygen-isotope variations in conodont apatite during diagenesis. *Geochimica et Cosmochimica Acta*, 210: 184-207.

Manuscript received 29 July 2026
Revised manuscript accepted 18 September 2026
Published online 28 September 2026
Editor Johannes Pignatti